



ELSEVIER

Contents lists available at ScienceDirect

## Materials Letters

journal homepage: [www.elsevier.com/locate/matlet](http://www.elsevier.com/locate/matlet)

# Amorphization of Nd–Fe–B alloy under the action of high-pressure torsion

B.B. Straumal<sup>a,b,c,d,\*</sup>, A.R. Kilmametov<sup>b</sup>, A.A. Mazilkin<sup>a,b</sup>, S.G. Protasova<sup>a,b</sup>,  
K.I. Kolesnikova<sup>a,c</sup>, P.B. Straumal<sup>c,e</sup>, B. Baretzky<sup>b</sup>

<sup>a</sup> Institute of Solid State Physics, Russian Academy of Sciences, Chernogolovka, Moscow district 142432, Russia

<sup>b</sup> Karlsruher Institut für Technologie, Institut für Nanotechnologie, Hermann-von-Helmholtz-Platz 1, 76344 Eggenstein-Leopoldshafen, Germany

<sup>c</sup> Laboratory of Hybrid Nanomaterials, National University of Science and Technology (MISIS), 119991 Moscow, Russia

<sup>d</sup> Moscow Institute of Physics and Technology (State University), 141700, Russia

<sup>e</sup> A.A. Baikov Institute of Metallurgy and Materials Science RAS, 117991 Moscow, Russia

## ARTICLE INFO

## Article history:

Received 26 November 2014

Accepted 13 January 2015

Available online 21 January 2015

## Keywords:

Phase transitions

Severe plastic deformation

Amorphization

Permanent magnets

## ABSTRACT

The high pressure torsion (HPT) has been used for the severe plastic deformation (SPD) treatment of liquid-phase sintered hard magnetic NdFeB-based alloy (5 GPa, 1 rpm, 5 torsions, ambient temperature). The amorphization of the crystalline alloy under the action of HPT has been observed. HPT permitted to obtain for the first time the mixture of two different amorphous phases with embedded grains of the ferromagnetic Nd<sub>2</sub>Fe<sub>14</sub>B phase. The SPD-treatment at ambient temperature  $T_{SPD}=300$  K is frequently equivalent to the heat treatment at a certain elevated temperature  $T_{eff} > 300$  K. The composition of phases in the studied NdFeB-based alloy after HPT corresponds to the state at  $T_{eff} \sim 1170$  °C.

© 2015 Elsevier B.V. All rights reserved.

## 1. Introduction

Since their discovery in 1980s the NdFeB-based alloys remain the best materials for permanent magnets [1]. It is due to their high spontaneous polarization  $J_S$ , Curie-temperature  $T_C$  and crystalline anisotropy  $K_1$  ( $J_S > 1.2$  T,  $T_C > 250$  °C,  $K_1 > 10^6$  J/m<sup>3</sup>) which ensures the excellent energy product  $(BH)_{max} > 450$  kJ/m<sup>3</sup> [2]. Therefore, the further development of these materials is still the important challenge for materials science [3]. The optimal microstructure of NdFeB-based alloys contains the (possibly fine) grains of the ferromagnetic Nd<sub>2</sub>Fe<sub>14</sub>B phase separated by the (possibly thin) non-magnetic layers (it is usually the Nd-rich phase) [3]. The main manufacture route of NdFeB-based permanent magnets is a liquid phase sintering of magnetically oriented powders [4]. Another route starts with a melt spinning which permits to obtain the nanograined structure or nanocrystals embedded in the amorphous phase [5]. Further the melt spun strips are compacted together or embedded in the polymer matrix. Nevertheless, the development of principally new methods for the production of NdFeB-based permanent magnets is extremely important. One of such methods is the severe plastic deformation (SPD) [6]. The idea of SPD is to deform the material in a confined space. It permits to increase the strain up to enormous values without fracture of a material. SPD

frequently leads to the phase transformations in the materials [7–10]. In other words, the phases before SPD and after this treatment are different. Thus, SPD can induce the dissolution of phases [11,12], formation [13] or decomposition [14] of a supersaturated solid solution, disordering of ordered phases [15], amorphization of crystalline phases [16,17], synthesis of the low-temperature [18], high-temperature [19] or high-pressure [20,21] allotropic modifications, and nanocrystallization in the amorphous matrix [22]. Quite frequently, the phases after SPD are the same as phases which would appear in a material after long anneal at a certain (elevated) temperature. This temperature is called effective temperature  $T_{eff}$ . SPD has been used for treatment of NdFeB-based alloys in several works [23–32]. The fine-grained or even nanograined microstructure has been observed after SPD of molten samples [23,24] or nanocrystallization in the amorphous matrix after SPD of melt-spun alloys [25–32]. In this work we report for the first time the direct amorphization of crystalline liquid-phase sintered NdFeB-based alloy under high pressure torsion (HPT). Also, the HPT drives the formation of a mixture of two different amorphous phases with embedded grains of the ferromagnetic Nd<sub>2</sub>Fe<sub>14</sub>B phase.

## 2. Experimental

The Nd–Fe–B-based liquid-phase sintered alloy was purchased from the company Vacuumschmelze GmbH (Germany): it contained 66.5 wt% Fe, 22.1 wt% Nd, 9.4 wt% Dy, 1.0 wt% Co, 0.8 wt% B, 0.2 wt% Cu. For HPT processing, the 0.6 mm thick discs were cut

\* Corresponding author at: Institute of Solid State Physics, Russian Academy of Sciences, Chernogolovka, Moscow district 142432, Russia. Tel.: +7 916 6768673; fax: +7 499 2382326.

E-mail address: [straumal@issp.ac.ru](mailto:straumal@issp.ac.ru) (B.B. Straumal).

from the as-cast ingots, then ground and chemically etched. The disks were subjected to HPT in a Bridgman anvil type unit (room temperature, pressure 5 GPa, 5 torsions, 1 rotation-per-minute) using a custom built computer controlled HPT device (W. Klement GmbH, Lang, Austria). After HPT, the central (low-deformed) part of each disk (about 3 mm in diameter) was excluded from further investigations. The samples for structural investigations were cut from the deformed disks at a distance of 4–5 mm from the sample centre. Scanning electron microscopy (SEM) investigations have been carried out in a Tescan Vega TS5130 MM microscope equipped with the LINK energy-dispersive spectrometer and on a Philips XL30 scanning microscope equipped with a LINK ISIS energy-dispersive spectrometer produced by Oxford Instruments. Transmission electron microscopy (TEM, HRTEM, STEM, EDXS) studies were carried out on the TITAN 60–300 instrument. X-ray diffraction (XRD) data were obtained on a Siemens diffractometer (Co K $\alpha$  radiation). Grain (crystallite) size was estimated by the XRD line broadening and using the Scherer formula.

### 3. Results and discussion

The torsion torque in the NdFeB-based alloy becomes stationary after about 2.5 anvil rotations. After quick starting increase of torsion torque from zero to  $\sim 250$  N m, the slow work hardening takes place. The torsion torque linearly increases till  $\sim 2.5$  anvil rotations. After this point the torsion torque stabilizes between 370 and 390 N m. The starting mixture of major Nd<sub>2</sub>Fe<sub>14</sub>B phase and some minor crystalline phases amorphizes during HPT (Fig. 1). XRD pattern in Fig. 1 clearly shows the amorphous halo and broad peaks of crystalline Nd<sub>2</sub>Fe<sub>14</sub>B and Fe phases. The width of XRD peaks permits to estimate the size of Nd<sub>2</sub>Fe<sub>14</sub>B and Fe crystallites below 10 nm. Z-contrast images obtained by HAADF STEM (Fig. 2a) show that HPT-treated samples contain areas of two different amorphous phases, namely Nd-rich (bottom side) and Fe-rich (top side). Fe-rich areas appear darker than Nd-rich ones. The line profile across the border between Fe-rich and Nd-rich area clearly shows the concentration difference. In the FFT from the HREM images (Fig. 2c–e) two different amorphous halos in the Nd-rich

area (Fig. 2c) and Fe-rich area (Fig. 2e) are clearly visible. Positions for the halos in Nd-rich and Fe-rich areas are different, which implies different composition of the corresponding amorphous phases. These halos overlap in the border between Nd-rich and Fe-rich areas (Fig. 2d). In the FFT from the HREM images (Fig. 2c–e) the diffraction spots from the Nd<sub>2</sub>Fe<sub>14</sub>B and Fe nanocrystallites are also present. The amorphous matrix contains the very fine Nd<sub>2</sub>Fe<sub>14</sub>B grains with size of 5–10 nm (Fig. 2a). These crystallites are the reason of fluctuations in the concentration profile of Fe and Nd (Fig. 2b)

TEM measurements show that the size of Fe-rich and Nd-rich amorphous areas are about 100–500 nm (Fig. 2). It means that during HPT at  $T_{SPD}=300$  K after  $t=300$  s the mass transfer on the distance  $L$  of at least 100 nm took place. In case of conventional bulk diffusion with coefficient  $D$  the distance  $L=(Dt)^{0.5}$ . Therefore, the equivalent diffusion coefficient  $D_{HPT}$  is about  $10^{-17}$  m<sup>2</sup>/s. In spite of the fact that high pressure slows down both bulk and GB diffusion [33,34], the  $D_{HPT}$  is many orders of magnitude higher than the values of  $D$  extrapolated to  $T_{SPD}$ . It means that, like in previously studied systems, HPT strongly accelerates mass transfer.

Thus, the strong external forces acting during HPT caused the phase transformation in the material, namely the formation of two different amorphous phases from crystalline ones and very strong refinement of Nd<sub>2</sub>Fe<sub>14</sub>B grains. Historically, such unusual behaviour was first observed in materials under severe irradiation [35]. G. Martin proposed for the first time a simplified mean-field description of solid solutions subjected to irradiation-induced atomic mixing [36]. His main idea was that the forced mixing induced by irradiation emulates the increase of entropy and changes the thermodynamic potentials in the alloy. G. Martin also proposed for the first time to use the equilibrium phase diagram for the description of the system under irradiation, but at  $T_{eff}$  instead of the actual temperature  $T$ . For example, if the liquid phase is present in the phase diagram at  $T_{eff}$ , the amorphous phase would appear under irradiation [36,37]. The composition of the phases after SPD allows to localize those phases in the respective equilibrium phase diagram (as we did previously for the Cu-based and Al-based alloys [10]) and to estimate the effective temperature  $T_{eff}$ . In case of NdFeB-based alloy HPT leads to the formation of two amorphous phases. The Nd–Fe–B phase diagram contains two immiscible melts above 1150 °C [38–40]. Therefore, the effective temperature is slightly above 1150 °C and can be estimated as  $T_{eff}=1170 \pm 30$  °C (Fig. 3, large filled circle). The transformation from crystalline state to amorphous one under SPD can also be considered as the solid-state reaction at the room temperature [41,42]. The formation of the mixture of two different amorphous phases from crystalline ones under the action of HPT has been observed for the first time in Ni–Nb–Y alloys [43]. In the Ni–Nb–Y alloys the regions of two different amorphous phases were very fine (few nm) and uniform mixed.

### 4. Conclusions

Severe plastic deformation by HPT leads to the phase transitions and strong grain refinement in several metallic alloys. SPD-treatment at ambient temperature  $T_{SPD}$  is frequently equivalent to the heat treatment at a certain elevated (effective) temperature  $T_{eff}$ . The steady-state is reached during HPT after a certain number of anvil rotations. The HPT of liquid-phase sintered hard magnetic NdFeB-based alloy permitted to obtain for the first time the mixture of two different amorphous phases with embedded grains of the ferromagnetic Nd<sub>2</sub>Fe<sub>14</sub>B and Fe phases. The composition of phases in the studied NdFeB-based alloy after HPT corresponds to the state at a certain effective temperature  $T_{eff} \sim 1170$  °C.

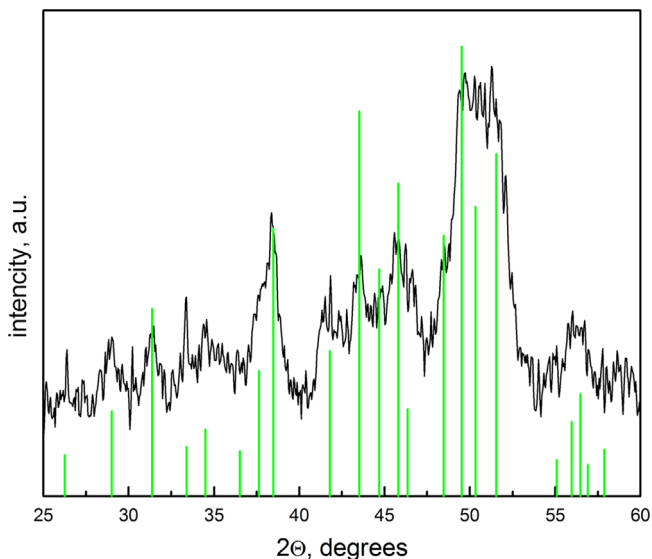
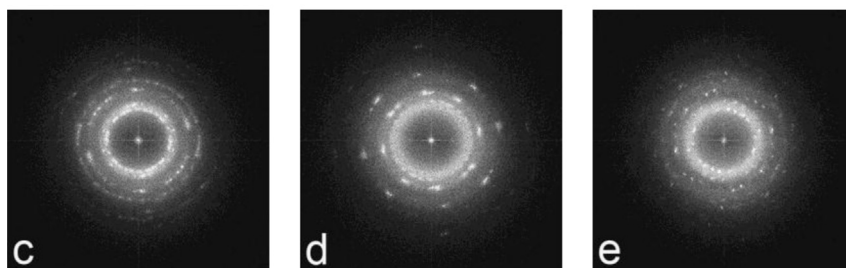
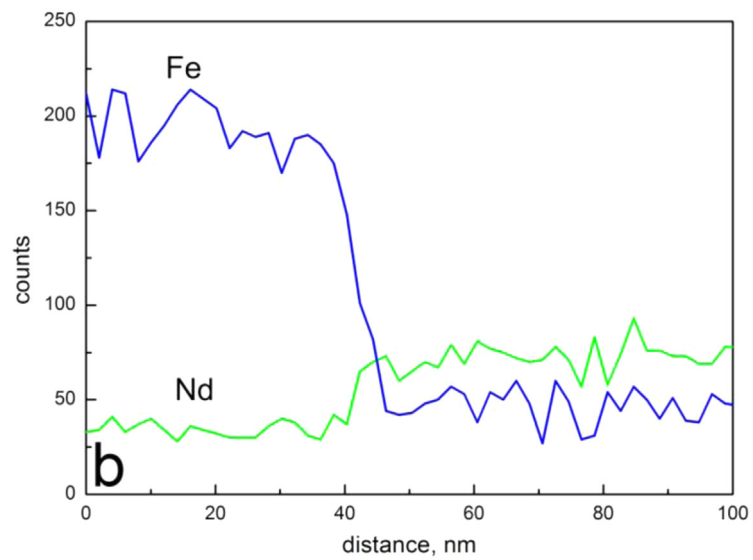
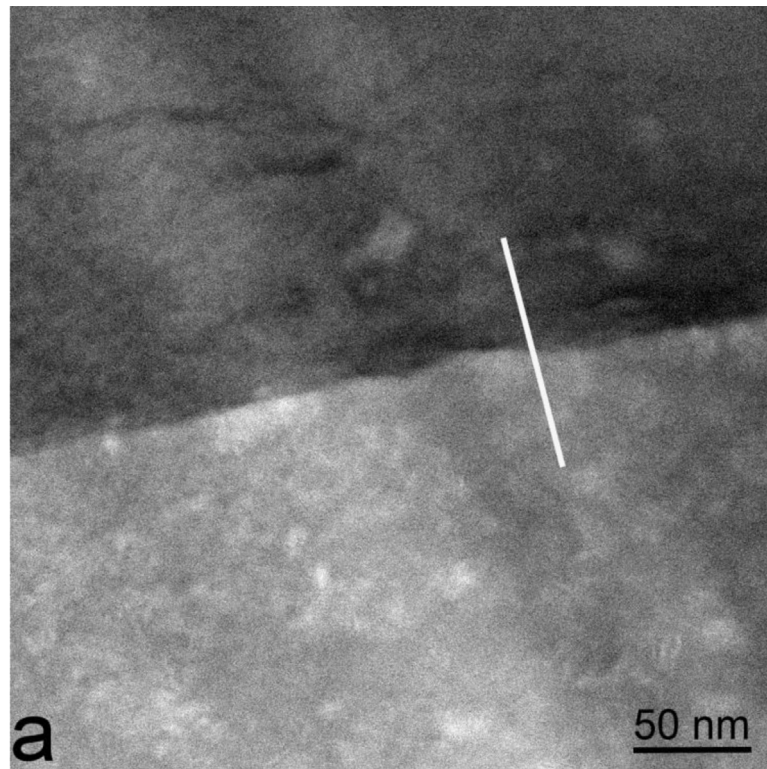


Fig. 1. XRD pattern of the Nd–Fe–B sample after HPT. The amorphous halo is visible under the main wide peak. The positions of the reflections from Nd<sub>2</sub>Fe<sub>14</sub>B phase are indicated by thin vertical lines.



**Fig. 2.** HAADF STEM image (a) of the Nd–Fe–B sample after HPT. Nd-rich and Fe-rich areas are distinguishable due to Z-contrast. Corresponding line profile along the white line in (a) also shows the variation of Nd and Fe content. FFT from the HREM images of the (c) Nd-rich area, (d) border between Nd-rich and Fe-rich areas and (e) Fe-rich area contains amorphous halos along with the crystalline reflections.

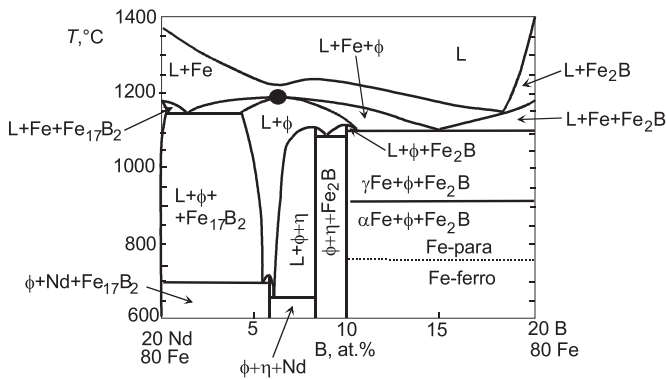


Fig. 3. The 80 at% Fe section of the Fe–Nd–B phase diagram [38–40]. Large filled circle shows the effective temperature  $T_{\text{eff}} = 1170 \pm 30$  °C.

### Acknowledgements

The work was partially supported by the Russian Foundation for Basic Research (Grants 15-03-01127, 14-48-03598 and 14-42-03621), Government of Moscow Region, Ministry of Education and Science of the Russian Federation in the framework of Increase Competitiveness Program of MISiS and for the Grant 14.A12.31.0001, Karlsruhe Nano Micro Facility, and the Allianz Industrie Forschung (Grant FE.5150.0028.4067).

### References

- [1] Schrefl T, Fidler J, Kronmüller H. *Phys Rev B* 1994;49:6100–10.
- [2] Rodewald W. Rare-earth transition-metal magnets. In: Kronmüller H, Parkin S, editors. *Handbook of magnetism and advanced magnetic materials*. Hoboken: John Wiley & Sons; 2007. p. 1969–2004.
- [3] Goll D, Kronmüller H. *Naturwiss* 2000;87:423–38.
- [4] Herbst JF. *Rev Mod Phys* 1991;63:819–98.
- [5] Manaf A, Buckley RA, Davies HA. *J Magn Magn Mater* 1993;128:302–6.
- [6] Valiev RZ, Islamgaliev RK, Alexandrov IV. *Prog Mater Sci* 2000;45:103–89.
- [7] Teitel' EI, Metlov LS, Gunderov DV, Korznikov AV. *Phys Met Metallogr* 2012;113:1162–8.
- [8] Sauvage X, Chbihi A, Quelenec X. *J Phys Conf Ser* 2010;240:012003.
- [9] Straumal BB, Sauvage X, Baretzky B, Mazilkin AA, Valiev RZ. *Scr Mater* 2014;70:59–62.
- [10] Straumal B, Korneva A, Zięba P. *Arch Civil Mech Eng* 2014;14:242–9.
- [11] Straumal BB, Dobatkin SV, Rodin AO, Protasova SG, Mazilkin AA, Goll D, et al. *Adv Eng Mater* 2011;13:463–9.
- [12] Sauvage X, Ivanisenko Y. *J Mater Sci* 2007;42:1615–21.
- [13] Sauvage X, Jessner P, Vurpillot F, Pippin R. *Scr Mater* 2008;58:1125–8.
- [14] Straumal BB, Baretzky B, Mazilkin AA, Philipp F, Kogtenkova OA, Volkov MN, et al. *Acta Mater* 2004;52:4469–78.
- [15] Korznikov AV, Tram G, Dimitrov O, Korznikova GF, Idrisova SR, Pakiela Z. *Acta Mater* 2001;49:663–71.
- [16] Prokoshkin SD, IYu Khmelevskaya, Dobatkin SV, Trubitsyna IB, Tatyaniy EV, Stolyarov VV, et al. *Acta Mater* 2005;53:2703–14.
- [17] Sauvage X, Renaud L, Deconihout B, Blavette D, Ping DH, Hono K. *Acta Mater* 2001;49:389–94.
- [18] Sagaradze VV, Shabashov VA. *Nanostruct Mater* 1997;9:681–4.
- [19] Yu Ivanisenko, Maclaren I, Sauvage X, Valiev RZ, Fecht H-J. *Acta Mater* 2006;54:1659–69.
- [20] Pérez-Prado MT, Zhilyaev AP. *Phys Rev Lett* 2009;102:175504.
- [21] Yu Ivanisenko, Kilmametov A, Rösner H, Valiev RZ. *Int J Mater Res* 2008;1:36–41.
- [22] Zs Kovács, Henits P, Zhilyaev AP, Révész Á. *Scr Mater* 2006;54:1733–7.
- [23] Stolyarov VV, Gunderov DV, Popov AG, Puzanova TZ, Raab GI, Yavari AR, et al. *J Magn Magn Mater* 2002;242:1399–401.
- [24] Popov AG, Gaviko VS, Shchegoleva NN, Puzanova TZ, Ermolenko AS, Stolyarov VV, et al. *Phys Metal Metallogr* 2002;94:575–81.
- [25] Li HL, Lou L, Hou FC, Guo DF, Li W, Li XH, et al. *Appl Phys Lett* 2013;14:142406.
- [26] Popov AG, Serikov VV, Kleinerman NM. *Phys Met Metallogr* 2010;109:505–13.
- [27] Li W, Guo DF, Li XH, Chen Y, Gunderov DV, Stolyarov VV, et al. *J Appl Phys* 2010;108:053901.
- [28] Li W, Li XH, Guo DF, Sato K, Gunderov DV, Stolyarov VV, et al. *Appl Phys Lett* 2009;94:231904.
- [29] Li W, Li LL, Nan Y, Xu ZY, Zhang XY, Popov AG, et al. *J Appl Phys* 2008;104:023912.
- [30] Popov AG, Gaviko VS, Shchegoleva NN, Shreder LA, Stolyarov VV, Gunderov DV, et al. *Phys Metal Metallogr* 2007;104:238–47.
- [31] Li W, Li LL, Nan Y, Li XH, Zhang XY. *Appl Phys Lett* 2007;91:062509.
- [32] Popov AG, Gaviko VS, Shchegoleva NN, Shreder LA, Gunderov DV, Stolyarov VV, et al. *J Iron Steel Res Int* 2006;13:160–5.
- [33] Straumal BB, Klinger LM, Shvindlerman LS. *Scr Met* 1983;17:275–9.
- [34] Molodov DA, Straumal BB, Shvindlerman LS. *Scr Met* 1984;18:207–11.
- [35] Sauvage X, Wilde G, Divinski SV, Horita Z, Valiev RZ. *Mater Sci Eng A* 2012;540:1–12.
- [36] Martin G. *Phys Rev B* 1984;30:1424–36.
- [37] Thomas G, Mori H, Fujita H. *Scr Met* 1982;16:589–92.
- [38] Ji ZS, Hu ML, Zheng XP. *J Mater Sci Technol* 2007;23:247–52.
- [39] Shatilla YA, Loewen EP. *Nucl Technol* 2005;151:239–49.
- [40] Sagawa M, Fujimura S, Togawa N, Yamamoto H, Matsuura Y. *J Appl Phys* 1984;55:2083–7.
- [41] Sundeep RV, Glezer AM, Shalimova AV. *Mater Lett* 2014;133:32–4.
- [42] Sundeep RV, Glezer AM, Shalimova AV. *J Alloys Compd* 2014;611:292–6.
- [43] Mazilkin AA, Abrosimova GE, Protasova SG, Straumal BB, Schütz G, Dobatkin SV, et al. *J Mater Sci* 2011;46:4336–42.